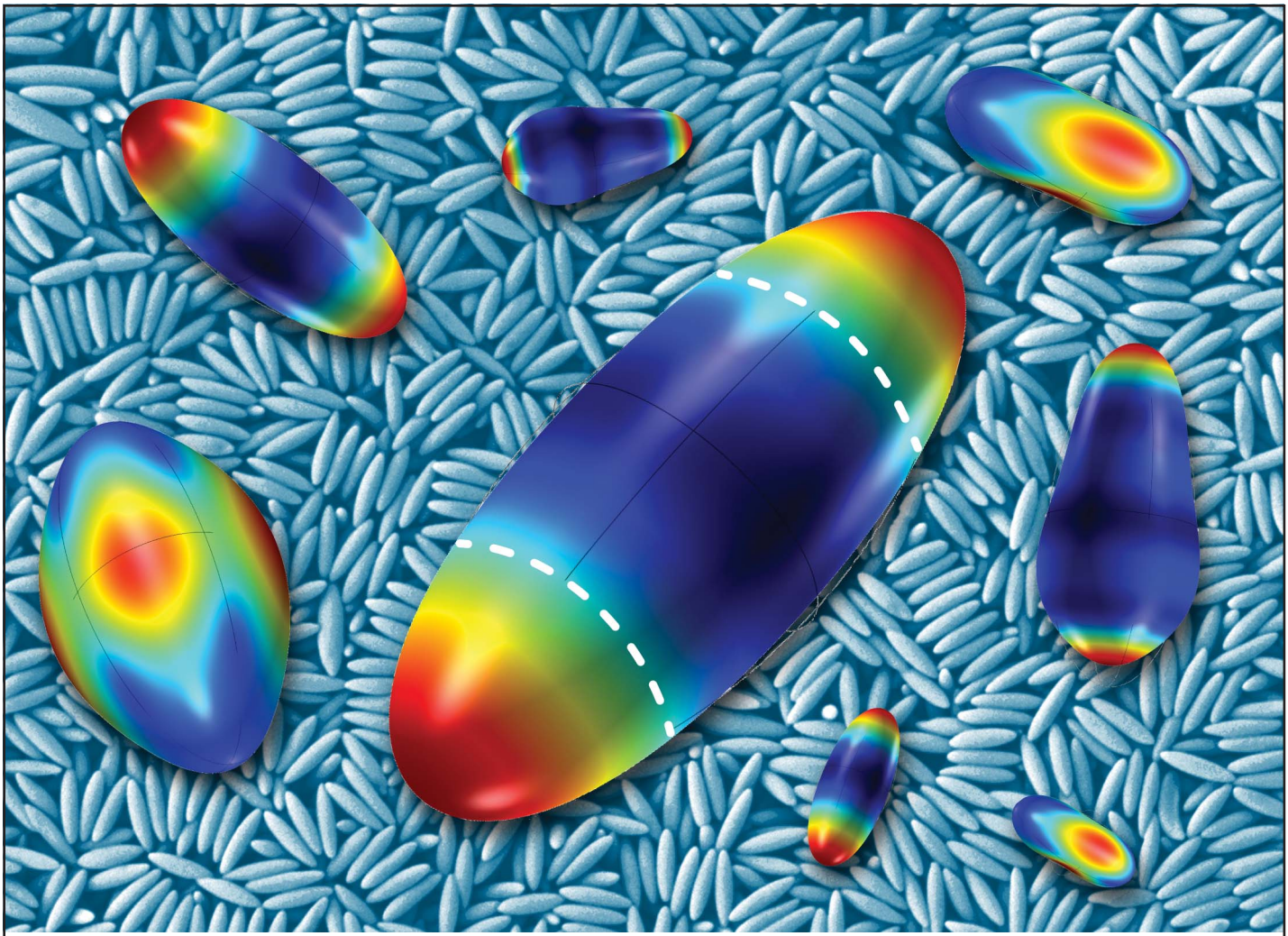

Highlighting joint research results from the Max Planck Institute for Polymer Research, University of Delaware, University of Trento, K.U. Leuven and the University of Crete and FORTH.

Title: Elongated polystyrene spheres as resonant building blocks in anisotropic colloidal crystals

Phononic properties of ordered assemblies of particles are strongly determined by the respective building blocks. The non-destructive technique of Brillouin light scattering resolves the vibrational eigenmodes of colloidal particles in analogy to the molecular vibration spectroscopy. For stretched polystyrene colloids, these fingerprints of shape, size and materials are represented by a single particle model.

As featured in:

See George Fytas *et al.*, *Soft Matter*, 2013, **9**, 9129.

RSC Publishing

www.rsc.org/softmatter

Registered Charity Number 207890

Soft Matter

RSC Publishing

PAPER

View Article Online
View Journal | View Issue

Cite this: *Soft Matter*, 2013, **9**, 9129

Elongated polystyrene spheres as resonant building blocks in anisotropic colloidal crystals†

Dirk Schneider,[a] Peter J. Beltramo,[b] Maurizio Mattarelli,[c] Patrick Pfleiderer,[d] Jan Vermant,[d] Daniel Crespy,[a] Maurizio Montagna,[c] Eric M. Furst[b] and George Fytas*[ae]

Received 7th April 2013
Accepted 31st May 2013

DOI: 10.1039/c3sm50959a

www.rsc.org/softmatter

Colloidal crystals have gained increasing importance due to their fascinating ability to mold the flow of light and sound (heat). The characteristics of these ordered assemblies of particles are strongly determined by the respective building blocks, which require complete understanding of their physical properties. In this study the mechanical properties of stretched polystyrene colloids (spheroids) are addressed. The non-invasive technique of Brillouin light scattering captures the vibrational spectra at hypersonic (GHz) frequencies. Resolved eigenmodes are considered fingerprints of the particles' shape, size and composing materials. A single particle model is used to simulate the experimental data by calculation of all active modes and subsequent evaluation of their contribution to the spectrum. Compared to spheres (high symmetry) more modes contribute to the spectra that limit the resolution at very high frequencies, due to the lifted mode degeneracy. Knowing the nature of the principal modes of spheroids is a precondition to understand the phononic dispersion in the respective colloidal crystals, in particular those responsible for anticrossing interactions with the effective medium acoustic phonon.

1 Introduction

In recent years, a vast library of colloidal building blocks has emerged from which novel materials may be created by directed self-assembly.[1–3] An open challenge to use directed self-assembly techniques in the nanomanufacture of complex materials with a designed functionality is the ability to (i) identify desired ordered structures to achieve such a functionality and (ii) develop efficient routes to manipulate the interparticle interaction energies to accomplish the assembly. To accomplish both goals, an understanding of the particle's physical properties is warranted.

Particular interest has emerged in the ordered assembly of ellipsoidal (spheroidal) particles due to the expanded range of final structures and additional flexibility in the design allowed by shape anisotropy. The self-assembly of spheroids has been examined at fluid interfaces[4,5] and using magnetic,[6,7] electric[8–10] or flow[11] fields. Specific to electric and magnetic fields, the anisotropy in polarizability along the short and long axes of an ellipsoid allows for preferential, tunable particle orientation ranging from parallel to perpendicular with the applied field.[12] Combining this orientational control with convective flows to concentrate the particles and "lock-in" the structure circumvents kinetic arrest that occurs at high volume fractions due to glassy dynamics and opens up the possibility of realizing the theoretically predicted close-packed phases of hard ellipsoids.[13,14] From a practical perspective, such structures may impart noteworthy photonic, phononic, mechanical and/or thermal properties to the resulting material due to alignment and periodicity. One recent example of the utility of controlling the orientational order of ellipsoidal particles was presented by Hopkins *et al.*,[15] where the thermal conductivity of convectively assembled titania films is modulated by the film microstructure.

At room temperature, thermal conductivity in dielectric materials relies mainly on phononic transport of energy in the sub-THz regime. Hence, direct access to the phononic dispersion becomes important. Brillouin spectroscopy has proven to be the tool of choice to investigate the phononic band diagram in the GHz range.[16] Colloidal crystals are of particular interest as they can accommodate both Bragg-type band gaps (due to destructive interference of elastic waves) and hybridization band gaps (due to level repulsion between the acoustic branch and a localized mode).[17] In the latter, the exact knowledge of a particle's eigenmode spectrum poses a substantial role. This

[a]*Max Planck Institute for Polymer Research, Ackermannweg 10, 55128 Mainz, Germany. E-mail: fytas@mpip-mainz.mpg.de*

[b]*Department of Chemical and Biomolecular Engineering, University of Delaware, Newark, DE 19716, USA*

[c]*Dipartimento di Fisica, Università di Trento, Via Sommarive 14, 38123 Trento, Italy*

[d]*Department of Chemical Engineering, K.U. Leuven, W. de Croylaan 46, B-3001 Leuven, Belgium*

[e]*Department of Materials Science, University of Crete and FORTH, 71110 Heraklion, Greece*

† Electronic supplementary information (ESI) available. See DOI: 10.1039/c3sm50959a

particle vibration spectroscopy based on Brillouin light scattering (BLS) becomes a valuable method for the mechanical characterization of sub-micron particles.[18] Eigenmode measurements have been reported for spheres,[18,19] nanorods,[20] cubes,[21,22] octahedra,[23,24] and more complex geometries[25,26] using BLS, Raman and time-resolved spectroscopy. While nanocolumns[27] were shown to shift the resonance line with respect to spherical particles, the eigenmode spectra of elongated spheres have not been fully investigated until now. Some of the aforementioned particles were synthesized from crystalline materials, whose anisotropic mechanical properties affect their eigenmodes in addition to the shape dependence.

Here we present a comprehensive particle vibration spectroscopy study of amorphous polystyrene (PS) spheres and spheroids (elongated spheres with rotational symmetry) utilizing the powerful technique of Brillouin light scattering combined with computational simulation of the spectra. To the best of our knowledge, this is the first work that provides theoretical representation for vibrational spectra of spheroidal nanoparticles studied by Brillouin spectroscopy.

2 Experimental

Polystyrene particles were stretched by a matrix assisted elongation process and the change of their eigenmode spectra was followed by Brillouin spectroscopy. The experimental strategy is outlined as follows:

2.1 Materials

The seed particles used were 400 nm diameter carboxylate modified PS latex spheres (Invitrogen, Eugene, OR, cat#C37238) with a molecular weight of $M_w \sim 240$ kDa. The spheroid synthesis procedure is described elsewhere.[28,29] In short, seed particles are dispersed in an aqueous poly(vinyl alcohol) (PVA) solution, spread in a dish and allowed to dry into a thin film after water evaporation. The film is then heated to 145 °C for less than 5 min (oil bath) and stretched to a given strain to produce 2.12 : 1, 3.52 : 1 and 3.99 : 1 aspect ratio prolate ellipsoids of revolution. The processed film was cut into small sections and cleaned from silicon oil by fivefold washing with isopropyl alcohol (IPA). The particles were recovered by dissolution in water/IPA 7 : 3 (v/v) and the suspensions are observed to be stable. These are washed *via* stirring (12 h), heating to 75 °C for one hour (to aid PVA removal), centrifugation, decantation and resuspension (sonication) in water/IPA. This cleaning cycle was repeated three times and finally the particles were stored in water. The suspensions were rewashed in 0.1 mM KCl and concentrated to a volume fraction $\phi \approx 0.05$ before being drop cast onto a glass slide and dried at ambient conditions.

The size of the particles is characterized by scanning electron microscopy of the disordered casts (Fig. 1) and a summary of the particle dimensions is given in Table 1.

2.2 Brillouin spectroscopy

Brillouin Light Scattering (BLS) serves as a non-destructive and non-contact technique to probe acoustic behavior, *e.g.*, thermally activated propagating phonons and localized vibration modes in the bulk as well as nanostructured materials in the hypersonic frequency regime (GHz). Hence, BLS is a sensitive tool to study the structure, morphology and light-matter interactions in composite materials, given that the phonon wavelength $2\pi/q$ commensurates their characteristic (periodic) spacing d, *i.e.*, $qd = \mathcal{O}(1)$. BLS relies on the interaction between single mode incident photons with wave vector $\boldsymbol{k}_i$ and thermally

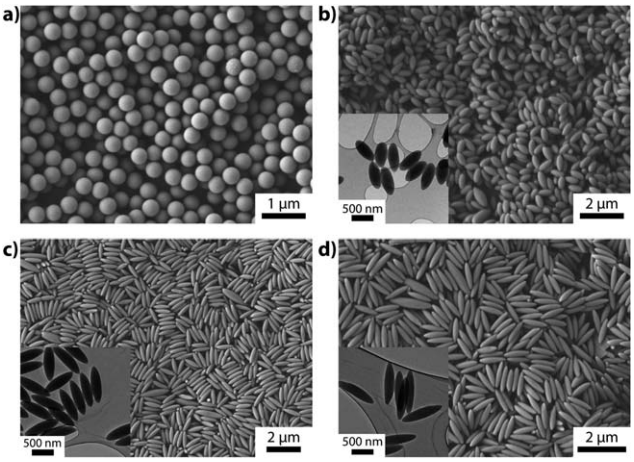

Fig. 1 Scanning electron micrographs (SEM) of seed spheres S0 (a) and spheroids S2–S4 (b–d) of various aspect ratios. Insets denote transmission images (TEM) of the respective particles.

Table 1 Size characterization of particles studied and material parameters used in calculations. a and b being the long and short axes of the spheroids, respectively. ρ is the mass density and n_{ref} the refractive index at 532 nm

ID	a/b	a/nm	b/nm	ρ/kg m^{-3}	n_{ref}[b]
S0	1	400 ± 14	_	1050	1.599
S1 (ref. 30)	1.28 ± 0.07	459 ± 15	358 ± 16	965.1[a]	1.540
S2	2.12 ± 0.16	690 ± 42	325 ± 15	921.9[a]	1.511
S3	3.52 ± 0.20	986 ± 15	280 ± 15	869.4[a]	1.477
S4	3.99 ± 0.22	1078 ± 93	270 ± 23	854.7[a]	1.468

[a] Calculated based on stretched particle volume. [b] Calculated from density *via* the Clausius–Mossotti relation.

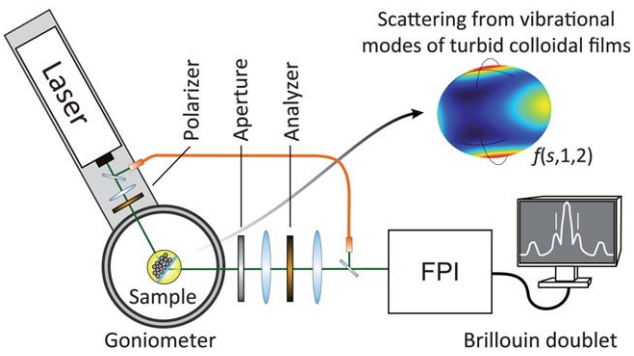

Fig. 2 Scheme of BLS instrumentation. A single-mode laser (532 nm) illuminates the turbid film and multiply scattered light is analyzed by a FP interferometer. The observed frequency shift represents the contribution of modes, e.g. $f(s,1,2)$, to the q-independent vibrational spectrum.

excited phonons $\boldsymbol{q} = \boldsymbol{k}_s - \boldsymbol{k}_i$ along a specified direction determined by the scattering geometry ($\boldsymbol{k}_s$ being the wave vector of the scattered photons). For localized modes in nanostructures, BLS gives a structured spectrum with contributions from all modes having a $\boldsymbol{q}$-component. In multiply scattering samples, $\boldsymbol{q}$ is no longer well-defined (the sample appears turbid) and hence all possible q-values contribute to the observed spectrum, regardless of which scattering angle θ is chosen. Realization of a high-resolution BLS experiment (Fig. 2) requires convenient and stable operation of an energy-dispersive detector. This is achieved using a six-pass tandem FP interferometer, which is actively stabilized by a reference beam and capable to detect a (anti-)Stokes shift of 0.5–300 GHz (*via* different free spectral ranges – FSR). A $\lambda = 532$ nm Nd/YAG laser mounted on a goniometer and a (heatable) cell holder allows for q-dependent and temperature dependent experiments.[17,31] Together, this setup provides the tool-kit necessary for high-resolution acoustic measurements at the nanoscale.

The typical accumulation time of the vibration spectrum in a drop cast powder-like film ranges from 30 to 120 min. Thin films or weakly scattering particles (size and material dependent) may require accumulation times up to 48 h.

BLS spectra obtained at $\theta = 60^\circ$ for the samples listed above (Table 1) were processed (stitched spectra at FSR = 7.5, 15, 30 GHz) and plotted in a common graph (Fig. 3). The upper panel (Fig. 3a) displays spectra for large changes in asphericity, from sphere up to an axis ratio of $a/b = 3.99$, while the lower panel (Fig. 3b) examines the small differences in the spectrum between the sphere (S0) and the particle with only slight elongation (S1).

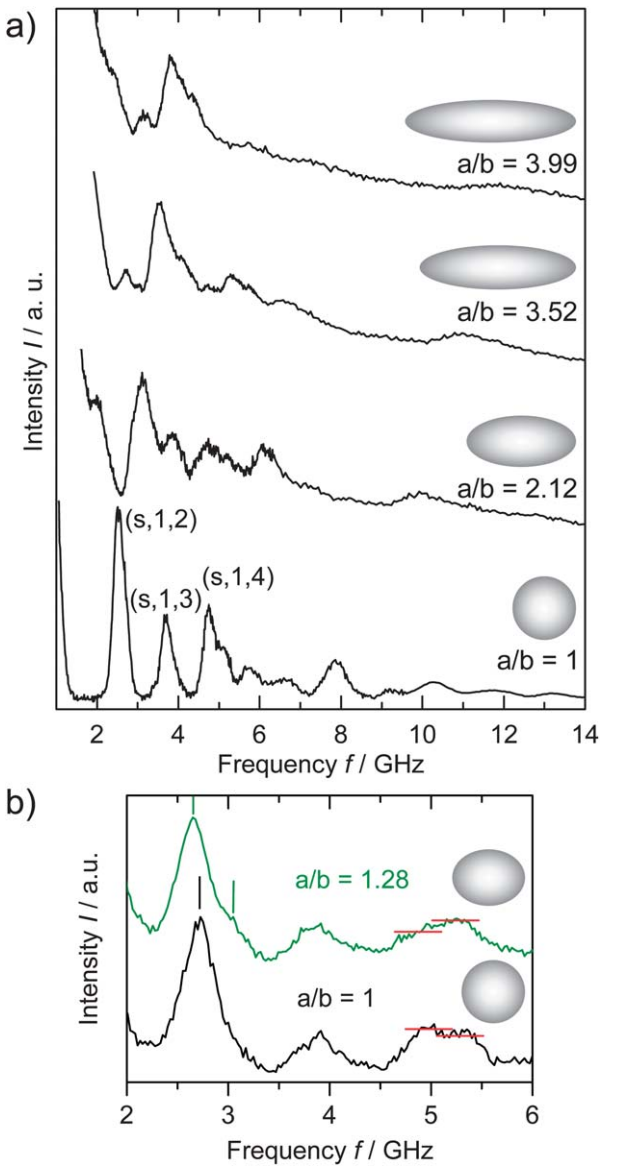

Fig. 3 (a) Brillouin light scattering (BLS) spectra of the spheroids with three different aspect ratios along with the rich spectrum of the seed spheres displaying the contribution of the principal modes (s,1,l = 2;3;4) in the low frequency region. (b) Onset of asphericity and the accompanying bifurcation of the lowest frequency (s,1,2) mode due to the lifting of degeneracy in m.

3 Theory

Propagating and localized acoustic modes in a medium induce fluctuations of the dielectric constant which can be probed by inelastic scattering of light. Limiting ourselves to the effect of density fluctuations, the contribution of the α-th mode, with frequency ω_α and $\boldsymbol{u}_\alpha$ displacements, to the scattered field in a one-phonon process was derived earlier.[32]

$$I_\alpha(\boldsymbol{q}) \propto \frac{n(\omega_\alpha, T) + 1}{\omega_\alpha} P^2 \left| \int_V \mathrm{e}^{-i\boldsymbol{q}\cdot\boldsymbol{x}} \boldsymbol{q}\cdot\mathbf{u}_\alpha(\boldsymbol{x})\, \mathrm{d}\boldsymbol{x} \right|^2, \qquad (1)$$

where $n(\omega_\alpha,T)$ is the Bose–Einstein factor, q is the exchanged wavevector, P is the polarizability density and the integral is over the volume V of the particle.

For spherical free homogeneous particles, the displacement field can be calculated following the theory developed by Lamb, using as parameters the sound velocities c_L and c_T and the size of the particle.[33] Within a continuum model, the normalized vibrational modes, $\boldsymbol{u}_\alpha$ are labeled by four indices, $\alpha \equiv (p,n,l,m)$. Torsional modes ($p = t$) have pure shear motions, whereas spheroidal modes ($p = s$) involve both shear and stretching. The n, l, m indices label the radial and angular vibrations of spheres in analogy to the atomic orbitals. For any l, we have $2l + 1$ modes whose Brillouin activity depends on the angle between the z-axis and the exchanged wavevector. The total intensity is anyway constant. Given the symmetry of the problem, it is possible to calculate it for an angle equal to zero, where the only active modes are those with cylindrical symmetry ($p = s$, $m = 0$). This procedure allowed reproducing the details of the particle vibration spectra with high sensitivity to the sound velocities.[18,34,35]

When we consider the light scattering induced from the vibrations of particles with different shapes, eqn (1) still holds once we have specified the displacements. The finite elements method (Comsol Multiphysics) was used to illustrate the displacements of two low-order modes for spheroid S2 with $m = 0$ (Fig. 4, right panel). The analytically calculated displacement for the two vibrational modes (s,1,2) and (s,1,3) are shown in the left panel of Fig. 4 and coincide with the numerical results.

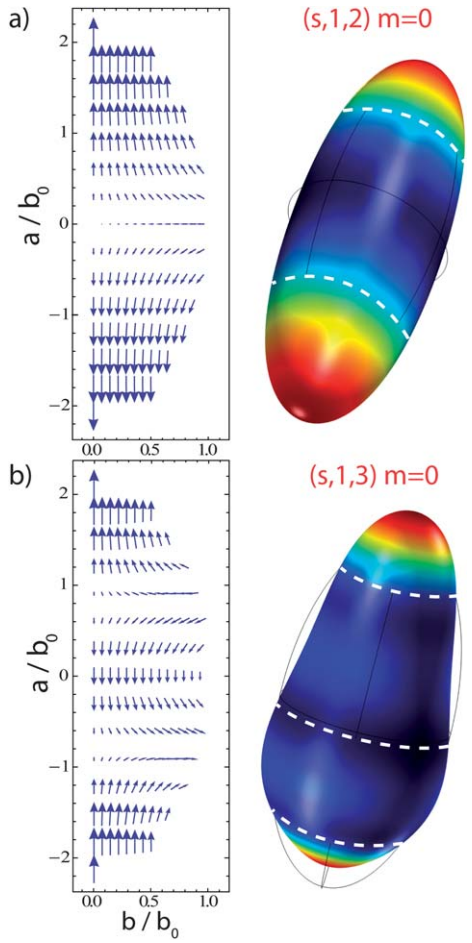

Fig. 4 Displacement fields of two low frequency modes commonly observed in Brillouin spectroscopy. The depicted aspect ratio corresponds to sample S2, with $a/b = 2.12$. (a) First $m = 0$ mode, mainly derived from (*s*,1,2), with two nodal lines (white dashes) and (b) second $m = 0$ mode, mainly derived from (*s*,1,3).

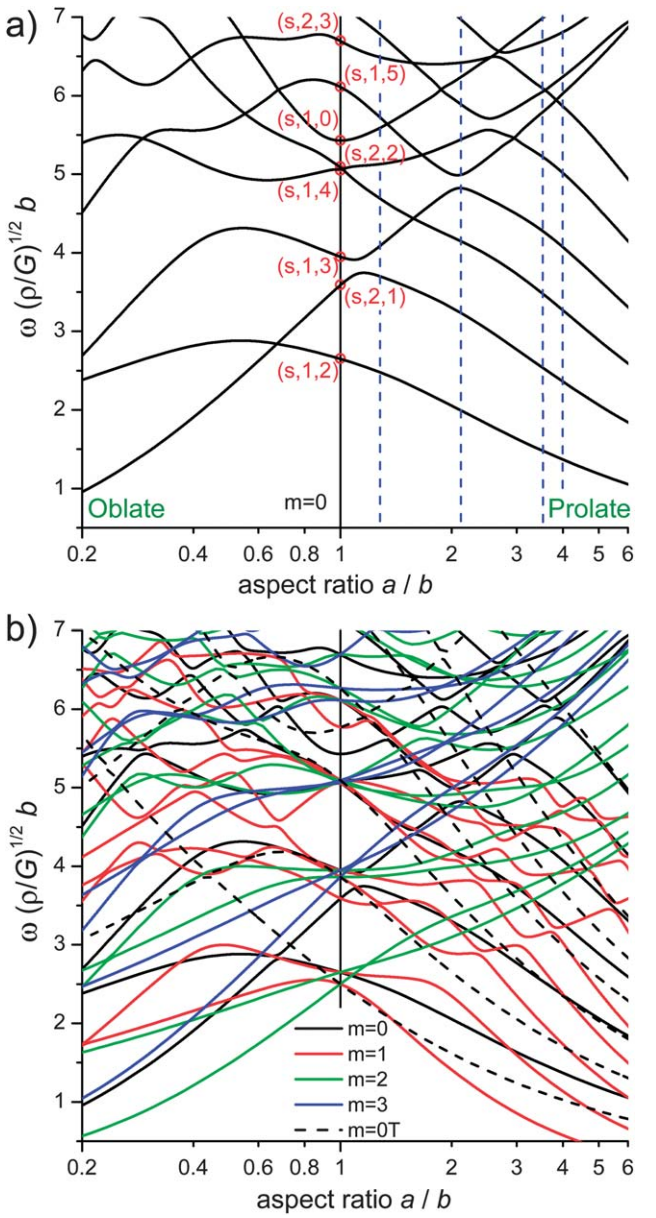

Fig. 5 (a) Adimensional frequency of the first vibrational modes as a function of the aspect ratio displayed for $m = 0$ only, for clarity. G is the shear modulus and ρ the density of the particle. (b) Additional bands shown for $m = 0,1,2,3$ as a function of the aspect ratio. For $m \neq 0$ no discrimination between torsional and spheroidal modes can be made, as both are active in BLS. Torsional modes (dashed lines) were calculated separately for $m = 0$, being non-active in BLS, as they produce no local dilatation.

A more precise displacement field of the vibrational modes is needed for the calculation of the Brillouin activity. This was achieved by following the procedure reported by Kang and Leissa, which considers the symmetry of the system.[36] The quantities needed for the calculation are the aspect ratio and the transverse and longitudinal sound velocities. The model has been validated comparing the results with those obtained by an analytical evaluation of the Lamb modes in a sphere. The mode frequencies and patterns show a very high agreement. Up to 7 GHz Brillouin spectra calculated from the two models are practically identical.

Fig. 5a shows the adimensional frequencies of the first vibrational modes as a function of the aspect ratio for a spheroid with fixed volume and $c_L/c_T = 1.96$. For clarity, only the modes with $m = 0$ are displayed. The blue dashed lines denote the aspect ratio of the particles under study. Fig. 5b shows the vibrational modes with m ranging from 0 to 3 for the same frequency range, whereas the dashed lines denote purely torsional modes, which are not Brillouin active. The solid vertical line marks the spherical case where the modes are degenerate in m. While for spherical particles we can assign (p,n,l,m) quantum numbers, as the axis ratio departs from 1 there is important mixing between the various modes of the sphere. For the spheroid vibrations l is no more a good quantum number and only for the aspect ratios close to 1 it is possible to identify modes with a dominant l number. In fact, the $(2l + 1)$ degeneracy in m of the (n,l) modes is lifted and we can discriminate the modes which correspond to $m = 0,1,2,3,\ldots$ Modes with opposite m $(n,l,\pm m)$ are still degenerate.

A detailed analysis of the complex behavior of modes dispersion is out of the scope of this paper. It is, however, relevant to note that crossing and anticrossing between the modes are present. Anticrossings which indicate a strong

mixing, show that the spheroid modes have no memory of the symmetry of the sphere modes from which they are derived apart from the m and the parity index. Note in particular that the torsional and spheroidal nature of the modes is not conserved. Only a subset of $m = 0$ modes are in fact torsional (with no local dilatation) and silent in the inelastic light scattering (dashed lines in Fig. 5b). All other modes present a stretching component and are active.

With increasing frequency the number of active modes increases (Fig. 5b) with concurrent decrease of their lifetime. These two facts lead to an increasing broadening of the vibration spectra of monodisperse spheroids with frequency. In addition, the inevitable presence of size/shape polydispersity renders the shape of the high frequency spectra featureless (Fig. 3a). Thus the low frequency regime of the BLS spectra becomes important for the determination of the thermomechanical properties of spheroidal particles with a large aspect ratio. In fact, for rods the only modes are the longitudinal (with displacement along the main axis and constant for any section), the bending (displacement perpendicular) and torsional ones.[25]

3.1 Simulation of Brillouin spectra

Having determined the displacement field for the vibrational modes of the spheroid, the Brillouin activity can be calculated by eqn (1). For a given mode, it will depend on the exchanged wavevector q and on the angle α between q and the main axis of the spheroid; note that differently from the sphere case, we cannot invoke symmetry in order to reduce ourselves to $\alpha = 0$. The studied samples show a significant turbidity which is the mark of the intense multiple scattering. In these conditions, we cannot consider a single exchanged q or α, even for aligned particles. The intensity has to be averaged on all angles between 0 and $\pi/2$ and all q's between 0 and $4\pi n_{ref}/\lambda$, where n_{ref} is the refractive index (Table 1) at the laser wavelength λ (=532 nm).

Operatively, we calculated frequency and displacements of the vibrational modes below 7 GHz of homogeneous spheroids with the aspect ratios of the samples in Table 1. The value of the Young's modulus and of the Poisson's ratio (and therefore of the velocity ratio) has been considered constant for all samples (S0–S4) being $E = 4.0$ GPa and $\nu = 0.32$ (corresponding to a velocity ratio c_L/c_T of about 2). However, the values of c_L and c_T are conceivable to change upon stretching[37] affecting also the density of the particles (Table 1). To a first approximation, the velocities scale with $\rho^{-1/2}$. The Brillouin activity was calculated on a grid of q and α values with steps of $1/3b$ and $\pi/16$ respectively. Discrete integration between 0 and $4\pi n_{ref}/\lambda$ and between 0 and $\pi/2$ with appropriate weights will produce the scattered intensity by any mode. Note, that for the stretched particles, the refractive index (Table 1) was evaluated using Clausius–Mossotti equation and considering that the polarizability of the scattering units has not changed after elongation. For a direct comparison with the experimental spectrum, the discrete calculated spectrum was broadened with Gaussian lineshapes. The latter take into account the experimental linewidth (0.25 GHz), the polydispersity in size ($\sigma_f/f = \sigma_d/d$) and the aspect ratio k ($\sigma_f = \partial f/\partial k \sigma_k$), with f denoting the vibrational frequency and σ the variance either in f or particle size d. This last source of broadening is very important for the lowest frequency $m = 1$ modes, whose frequency is strongly dependent on the aspect ratio as shown in Fig. 5. One effect of line broadening is a shift of the peaks toward lower frequency with respect to the average position calculated for the mean values, as it clearly appears for the low frequency peaks of Fig. 3b. It is caused by the $(n(\omega,T) + 1)/\omega$ term of eqn (1), which favors particles with larger size and aspect ratio.

Here, we point out that all calculations were performed using no fitting parameters. Furthermore, no anisotropy of elastic properties was regarded along the two axes. Mechanical anisotropy induced by the elongation process would be a conceivable source of broadening.[38] AFM assisted fractal analysis of the surface texture is a conceivable method to identify ordering modification (due to chain elongation) in the stretched particles.[39] However, this method is not applicable when using a sacrificial PVA matrix. Although mild, processing modifies the surface structure with regard to topography, charge and residual PVA.

4 Results and discussion

In order to check the accuracy, the simulation procedure was applied to the spherical particles before (untreated) and after (treated) embedding them in the PVA. The agreement (Fig. 6) is quite good and comparable to earlier results for spheres.[18] Note,

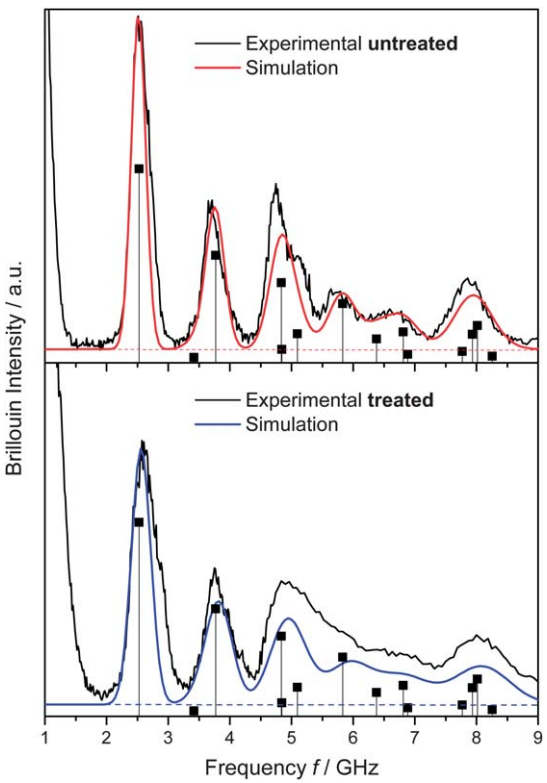

Fig. 6 Brillouin spectra and simulation of spheres, before (upper panel) and after (lower panel) embedding in the PVA matrix. Recovered particles exhibit reduced volume and larger size dispersion.

that the fitting of the treated sample (blue line in Fig. 6) has been made considering a larger size polydispersity ($\sigma_d/d = 0.06$ *vs.* 0.035 in the untreated) and a decreased volume (6%), resulting from the removal of the PVA matrix. The vibrational spectrum in particular at low frequencies seems to be very sensitive to size/shape changes even after mild processing conditions.

Clearly, processing is able to modify the particle identity, as monitored by BLS. This change of spectral shape exemplifies the sensitivity to surface fluctuations which is induced by the stretching process. While the shift of frequencies due to size decrease or a mixed PVA/PS surface layer can be attributed to the etching process, the observed broadening does not have such a clear attribution. In the fit it has been considered by increasing the size dispersion, but it could also be due to a departure from spherical symmetry. Furthermore, it should be noted that a single particle model has been considered neglecting the (possibly increased) interaction between neighboring particles, which causes a line broadening.[34] Finally the particles were considered homogeneous with no density gradient near the surface, a possible result of the mild processing.

As the particle shape departs from spherical symmetry the degeneracy in m is lifted and more modes contribute to the spectrum. This reduced symmetry[24] and to a lesser degree mechanical anisotropy[38] cause the spectral features to be washed out at higher frequency, in addition to size/shape polydispersity. An aspect ratio of 1.28 (Fig. 3b) is already large enough that the distinction, found in parent spheres, between torsional and spheroidal modes is no longer valid. Therefore any peak is in fact the sum of several contributions with different m. In Fig. 7 the first peak at 2.65 GHz can be considered as the sum of the m-split (s,1,2) mode of the parent sphere and causes the broadening, even if the contribution from $m = 1$ (red) and $m = 2$ (green) modes derived from the (t,1,2) Lamb mode is not negligible. The situation for the peak at 5 GHz is even more complicated as it consists of many contributions already in the parent sphere. The swapped intensity between the two shoulders (red horizontal lines in Fig. 3b) is just a consequence of the manifold shift of lines.

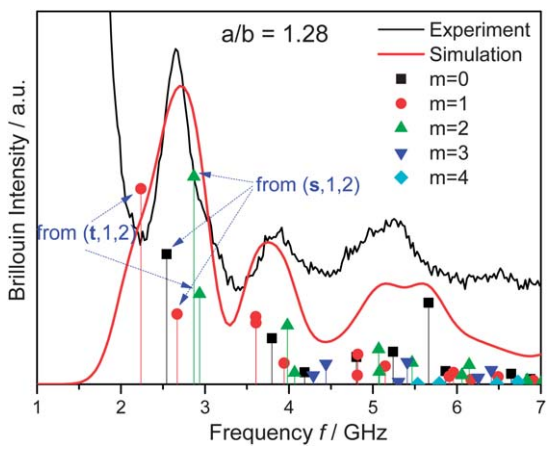

Fig. 7 Brillouin spectra for relatively low asphericity ($a/b = 1.28$). The shift of spheroidal and torsional lines (blue arrows) cause significant broadening of the low-frequency peak.

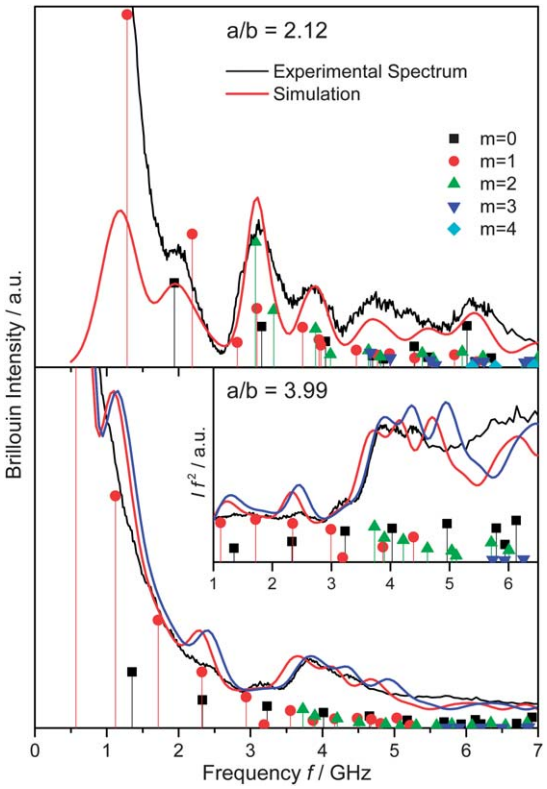

Fig. 8 Brillouin spectra for spheroids of aspect ratio 2.12 (upper panel) and 3.99 (lower panel). The inset to the lower panel displays the reduced spectrum for S4. Theoretical Brillouin intensity (red lines) as calculated from the sum of the individual contributions $m = 0, \ldots, 4$ (modes with $m > 4$ have frequencies higher than 7 GHz). Sources of broadening are the instrumental resolution as well as size and shape dispersion of the spheroids. The blue line in the lower panel gives the simulation with 6% increased sound velocity.

In order to follow this transition trend from homogeneous spheres towards an homogeneous rod, we examined higher aspect ratios. Fig. 8 (upper panel) displays the superposition of experimental and simulated spectra for sample S2 ($a/b = 2.12$). Peak positions and relative intensity are well represented. Sound velocities larger than that of PS were used to account for the reduced density at constant elastic constants *via* $M,G = \rho c^2_{L,T}$, M (G) being the longitudinal (shear) modulus.

At very low frequencies the flanks of the elastic line disturb the inspection of the lower order peaks (*e.g.*, for $m = 1$). In a reduced plot (Fig. S1, upper panel)† the low-frequency contribution at about 1.3 GHz, which is not observed in Fig. 8, is clearly resolved. Due to experimental restrictions (lowest free spectral range and in particular the strong elastic line) frequencies below ~1 GHz were not accessible.

As the aspect ratio is increased (bottom panel of Fig. 8) the agreement of simulation and experimental spectra isn't as good as for $a/b = 2.12$. Possibly, the mechanical anisotropy introduced by the stretching process to achieve high aspect ratios cannot be neglected anymore. The modes contributing to the spectrum are too many to be observed individually. The peaks appear much more broadened than those of the upper panel. A

broad peak at about 2.5 GHz seems to be reproduced by a couple of nearly resonant modes, the 4th $m = 1$ and the 2nd $m = 0$. It better appears in the reduced spectrum (inset to Fig. 8), that is obtained by multiplying the experimental spectrum by f^2. The calculated spectrum reproduces well the sharp increase of the intensity occurring at about 3.5 Ghz, which is attributed to several different modes. The representation of the spectrum for $a/b = 3.99$ using sound velocity values adjusted to the density is of moderate quality (red line). Instead, a further increase ($\sim$6%) of the sound velocities, while keeping constant their ratio (c_L/c_T) leads to better agreement with the experimental spectrum (blue line in Fig. 8) as without any adjustable parameter (red line). This hardening in stretched polymers has been reported before[40] and reflects the mechanical anisotropy caused by the stretching process. Only for the particles with the largest aspect ratio, the moduli increase by about 12% compared to the spherical parent particles. For the particles with lower aspect ratio, it is worth mentioning the insensitivity of the average moduli and hence the Poisson's ratio to the stretching of the PS spheres. This preserved mechanical strength is an unprecedented information from the particle vibrational spectra.

5 Conclusions

This work presents the capability of a computational method combined with Brillouin spectroscopy as an effective tool for the characterization of the elastic properties of elongated spheres. Notwithstanding the significant approximation involved we were able to reproduce reasonably well the experimental spectra of spheroidal particles. However, a few obstacles are faced with respect to the results for the spherical particles: (i) the m-splitting of the modes, which multiplies any sphere (n,l) mode into $l + 1$ ones at different frequencies and (ii) the polydispersity of the samples (size and aspect ratio). The mixed effect of increasing the number of active modes and of the polydispersity induced broadening leads to practically featureless spectra for frequencies higher than $\sim$7 GHz (Fig. 3a). In any case the apparent peaks in the Brillouin spectra are indeed the sum of many different contributions (*e.g.*, the peak at $\sim$4 GHz in the spectrum of sample S4 is the sum of 7 peaks of comparable intensities).

From the good theoretical representation of the experimental vibration spectra, all four but the highest aspect ratio spheroidal PS particles preserve the same orientation averaged elastic constants with the seed spheres while the density (sound velocity) decreased (increased) with asphericity. The highest aspect ratio ($a/b \sim 4$) spheroids possess elastic moduli increased by 12%. As an outlook, the low frequency vibrational spectrum can be also utilized to assess the thermomechanical properties and determine the glass transition temperature of these spheroids through a temperature dependent study and establish the analogy to the spherical particles.[34]

This knowledge can be used for the study of phononic properties of an ordered assembly. The opening of hybridization gaps requires strong localization of elastic energy in the building units.[17] It becomes even more important, as energy leakage is allowed when the local resonator is placed in a liquid to assure optical matching.[41] For spheroids, mostly the rather well separated vibrational states in the low-frequency regime will play a major role for anticrossing interaction with the acoustic branch, *i.e.* opening of hybridization gaps. Colloidal crystals with spheroidal building blocks will exhibit inherently anisotropic mechanical and optical properties. Hence, thermal conductivity as well as transmission of light and sound will be a function of the orientation relative to the asymmetric particles.

Acknowledgements

The authors like to thank Christine Herrmann for providing the low-asphericity samples ($a/b = 1.28$) and Kathryn Whitaker for taking the TEM images. This work was supported by DFG (BU 1556/27) and ARISTEIA Program-285 (EU, GSRT-Greece). PJB and EMF acknowledge support from the U.S. Department of Energy, Office of Basic Energy Sciences, Division of Materials Sciences and Engineering under Award no. DE-FG02-09ER46626.

References

1 M. Grzelczak, J. Vermant, E. M. Furst and L. M. Liz-Marzan, *ACS Nano*, 2010, **4**, 3591–3605.
2 S. Sacanna and D. J. Pine, *Curr. Opin. Colloid Interface Sci.*, 2011, **16**, 96–105.
3 S. C. Glotzer and M. J. Solomon, *Nat. Mater.*, 2007, **6**, 557–562.
4 B. Madivala, J. Fransaer and J. Vermant, *Langmuir*, 2009, **25**, 2718–2728.
5 Z. Zhang, P. Pfleiderer, A. B. Schofield, C. Clasen and J. Vermant, *J. Am. Chem. Soc.*, 2011, **133**, 392–395.
6 T. Ding, K. Song, K. Clays and C.-H. Tung, *Adv. Mater.*, 2009, **21**, 1936–1940.
7 T. Ding, K. Song, K. Clays and C.-H. Tung, *Langmuir*, 2010, **26**, 11544–11549.
8 J. P. Singh, P. P. Lele, F. Nettesheim, N. J. Wagner and E. M. Furst, *Phys. Rev. E: Stat., Nonlinear, Soft Matter Phys.*, 2009, **79**, 050401.
9 M. Mittal and E. M. Furst, *Adv. Funct. Mater.*, 2009, **19**, 3271–3278.
10 A. A. Shah, H. Kang, K. L. Kohlstedt, K. H. Ahn, S. C. Glotzer, C. W. Monroe and M. J. Solomon, *Small*, 2012, **8**, 1551–1562.
11 M. Mittal, R. K. Niles and E. M. Furst, *Nanoscale*, 2010, **2**, 2237–2243.
12 T. B. Jones, *Electromechanics of Particles*, Cambridge University Press, 1995.
13 P. Pfleiderer and T. Schilling, *Phys. Rev. E: Stat., Nonlinear, Soft Matter Phys.*, 2007, **75**, 020402.
14 A. Donev, F. H. Stillinger, P. M. Chaikin and S. Torquato, *Phys. Rev. Lett.*, 2004, **92**, 255506.
15 P. E. Hopkins, M. Mittal, L. M. Phinney, A. M. Grillet and E. M. Furst, *Appl. Phys. Lett.*, 2011, **99**, 133106.
16 W. Cheng, J. Wang, U. Jonas, G. Fytas and N. Stefanou, *Nat. Mater.*, 2006, **5**, 830–836.
17 T. Still, W. Cheng, M. Retsch, R. Sainidou, J. Wang, U. Jonas, N. Stefanou and G. Fytas, *Phys. Rev. Lett.*, 2008, **100**, 194301.

18 T. Still, M. Mattarelli, D. Kiefer, G. Fytas and M. Montagna, *J. Phys. Chem. Lett.*, 2010, **1**, 2440–2444.
19 T. Still, M. Retsch, U. Jonas, R. Sainidou, P. Rembert, K. Mpoukouvalas and G. Fytas, *Macromolecules*, 2010, **43**, 3422–3428.
20 M. Hu, X. Wang, G. V. Hartland, P. Mulvaney, J. P. Juste and J. E. Sader, *J. Am. Chem. Soc.*, 2003, **125**, 14925–14933.
21 H. Petrova, C.-H. Lin, S. de Liejer, M. Hu, J. M. McLellan, A. R. Siekkinen, B. J. Wiley, M. Marquez, Y. Xia, J. E. Sader and G. V. Hartland, *J. Chem. Phys.*, 2007, **126**, 094709.
22 J. Y. Sun, Z. K. Wang, H. S. Lim, S. C. Ng, M. H. Kuok, T. T. Tran and X. Lu, *ACS Nano*, 2010, **4**, 7692–7698.
23 H. H. Pan, Z. K. Wang, H. S. Lim, S. C. Ng, V. L. Zhang, M. H. Kuok, T. T. Tran and X. M. Lu, *Appl. Phys. Lett.*, 2011, **98**, 133123.
24 B. Stephanidis, S. Adichtchev, S. Etienne, S. Migot, E. Duval and A. Mermet, *Phys. Rev. B: Condens. Matter Mater. Phys.*, 2007, **76**, 121404.
25 M. Pelton, J. E. Sader, J. Burgin, M. Liu, P. Guyot-Sionnest and D. Gosztola, *Nat. Nanotechnol.*, 2009, **4**, 492–495.
26 H. Portalès, N. Goubet, L. Saviot, P. Yang, S. Sirotkin, E. Duval, A. Mermet and M.-P. Pileni, *ACS Nano*, 2010, **4**, 3489–3497.
27 J. Margueritat, J. Gonzalo, C. N. Afonso, A. Mlayah, D. B. Murray and L. Saviot, *Nano Lett.*, 2006, **6**, 2037–2042.
28 C. Ho, A. Keller, J. A. Odell and R. H. Ottewill, *Colloid Polym. Sci.*, 1993, **271**, 469–479.
29 K. M. Keville, E. I. Franses and J. Caruthers, *J. Colloid Interface Sci.*, 1991, **144**, 103–126.
30 C. Herrmann, M. B. Bannwarth, K. Landfester and D. Crespy, *Macromol. Chem. Phys.*, 2012, **213**, 829–838.
31 R. S. Penciu, H. Kriegs, G. Petekidis, G. Fytas and E. N. Economou, *J. Chem. Phys.*, 2003, **118**, 5224–5240.
32 M. Montagna, *Phys. Rev. B: Condens. Matter Mater. Phys.*, 2008, **77**, 045418.
33 H. Lamb, *Proc. London Math. Soc.*, 1882, **13**, 189–212.
34 M. Mattarelli, M. Montagna, T. Still, D. Schneider and G. Fytas, *Soft Matter*, 2012, **8**, 4235–4243.
35 M. Mattarelli and M. Montagna, *Chem. Phys. Lett.*, 2012, **524**, 112–115.
36 J.-H. Kang and A. Leissa, *Acta Mech.*, 2008, **197**, 97–117.
37 N. Gomopoulos, G. Saini, M. Efremov, P. F. Nealey, K. Nelson and G. Fytas, *Macromolecules*, 2010, **43**, 1551–1555.
38 L. Saviot and D. B. Murray, *Phys. Rev. B: Condens. Matter Mater. Phys.*, 2009, **79**, 214101.
39 D. Konopinski, S. Hudziak, R. Morgan, P. Bull and A. Kenyon, *Forensic Sci. Int.*, 2012, **223**, 245–255.
40 M. Sinha, B. Erman, J. E. Mark, T. H. Ridgway and H. E. Jackson, *Macromolecules*, 2003, **36**, 6127–6134.
41 T. Still, G. Gantzounis, D. Kiefer, G. Hellmann, R. Sainidou, G. Fytas and N. Stefanou, *Phys. Rev. Lett.*, 2011, **106**, 175505.